Benchmark calculation of the three-nucleon photodisintegration

- J. Golak^{1,2}, R. Skibiński², W. Glöckle¹, H. Kamada³, A. Nogga⁴, H. Witała²

 ¹ Institut für Theoretische Physik II, Ruhr-Universität Bochum, D-44780 Bochum, Germany

 ² Institute of Physics, Jagellonian University, PL-30059 Cracow, Poland

 ³ Department of Physics, Faculty of Engineering, Kyushu Institute of Technology

 1-1 Sensucho, Tobata, Kitakyushu 804-8550, Japan

 ⁴ Department of Physics, University of Arizona, Tucson, Arizona 85721, USA
- V. D. Efros⁵, W. Leidemann⁶, G. Orlandini⁶ and E.L. Tomusiak⁷

 ⁵ Russian Research Centre "Kurchatov Institute", Kurchatov Square 1, 123182 Moscow, Russia

 ⁶ Dipartimento di Fisica, Università di Trento and INFN (Gruppo collegato di Trento)

 I-38050 Povo (Trento), Italy

 ⁷ Department of Physics and Astronomy, University of Victoria, Victoria BC V8P 1A1, Canada

(October 29, 2018)

Abstract

A benchmark is set on the three–nucleon photodisintegration calculating the total cross section with modern realistic two– and three–nucleon forces (AV18, UrbIX) using both the Faddeev equations and the Lorentz Integral Transform method. This test shows that the precision of three-body calculations involving continuum states is considerably higher than experimental uncertainties. Effects due to retardations, higher multipoles, meson exchange currents and Coulomb force are studied.

PACS: 21.45.+v, 25.20.Dc

Keywords: few-body, photoabsorption, Faddeev equations, Lorentz Integral Transform

I. INTRODUCTION

The total photodisintegration cross sections of the three–body nuclei are important quantities for understanding electromagnetic processes in nuclei. Several approximate theoretical calculations have been performed in the past with simple NN-potential models [1–4]. The first calculations with complete final state interaction were carried out with the Lorentz Integral Transform (LIT) method using semirealistic [5] and realistic NN and 3N forces [6,7]. In this paper we intend to set a benchmark on the results of the three–nucleon total photodisintegration by calculating the cross section with modern realistic two– and three–nucleon forces. To this end we use two different methods, namely the Faddeev and the LIT approaches. On the one hand the comparison between the results gives an idea of the precision reached by three-body calculations involving continuum states while on the other hand it may stimulate more accurate measurements.

It has long been believed that the photonuclear cross section is dominated by unretarded dipole transitions. The contributions of magnetic and higher order electric multipoles, of retardation, as well as of meson exchange currents have been discussed extensively. However, rigorous results have only been given for the deuteron [8–10]. In this paper we give for the first time a quantitative discussion of these issues for the three-body nuclei.

The paper is organized as follows. In Sec. 2 we briefly summarize the two methods for obtaining the total photodisintegration cross section. In Sec. 3 we present the comparison between the two calculations and discuss the effects of the Coulomb force, as well as the contributions beyond the unretarded dipole operator. Conclusions are drawn at the end.

II. THEORETICAL FRAMEWORK

The total unpolarized photodisintegration cross section is given by

$$\sigma_T(E_\gamma) = R_T(E_\gamma) \frac{1}{E_\gamma} 4\pi^2 \frac{e^2}{\hbar c} \,. \tag{1}$$

In terms of the matrix elements of the transverse current operator $\mathbf{J_T}$ the transverse response function $R_T(E_{\gamma})$ is

$$R_T(E_\gamma) = \int df |\langle \Psi_f | \mathbf{J_T} | \Psi_0 \rangle|^2 \delta(E_\gamma - E_f + E_0 - \frac{E_\gamma^2}{2M_t}), \qquad (2)$$

where Ψ_0 is the three–nucleon bound state wave function with energy E_0 , and Ψ_f are final state wave functions. The term $E_{\gamma}^2/(2M_t)$ in the energy conserving delta–function represents the small recoil energy of the whole 3–body nucleus with mass M_t . In the following subsections it is described how R_T is calculated using the Faddeev equations and the LIT method.

A. The Faddeev equations

The way the transverse response function R_T is calculated in the Faddeev framework for inclusive electron scattering without a 3N force is described in Refs. [11] and [12]. Here we

sketch the corresponding derivation for the case when a 3N force is additionally taken into account.

For a general operator \mathcal{O} and using closure the function in Eq. (2) is rewritten as

$$R_{\mathcal{O}}(E_{\gamma}) = -\frac{1}{\pi} \Im \langle \Psi_0 | \mathcal{O}^{\dagger} \frac{1}{E + i\epsilon - H} \mathcal{O} | \Psi_0 \rangle, \qquad (3)$$

where $E = E_0 - E_{\gamma}^2/(2M_t) + E_{\gamma}$ and H is the 3N Hamiltonian. Next we define an auxiliary state

$$|\Psi\rangle \equiv \frac{1}{E + i\epsilon - H} \mathcal{O}|\Psi_0\rangle \,,$$
 (4)

which fulfils the following equation

$$(E + i\epsilon - H) |\Psi\rangle = \mathcal{O}|\Psi_0\rangle. \tag{5}$$

This leads to an intermediate equation

$$|\Psi\rangle = G_0 (V_1 + V_2 + V_3 + V_4) |\Psi\rangle + G_0 \mathcal{O} |\Psi_0\rangle.$$
 (6)

Here V_i is the NN potential (we use the notation $V_1 = V_{23}$ etc.), V_4 is a 3N force and G_0 the free 3N propagator. Both the operator \mathcal{O} and the 3N force V_4 can be written as a sum of three parts having the same symmetry under particle exchanges.

$$\mathcal{O} = \sum_{i=1}^{3} \mathcal{O}_{i}, \qquad (7)$$

$$V_{4} = \sum_{i=1}^{3} V_{4}^{(i)}$$

Introducing the Faddeev decomposition of the state $|\Psi\rangle$

$$|\Psi\rangle = G_0 \sum_{i=1}^{3} |U_i\rangle \tag{8}$$

we obtain from Eq. (6) (for three identical nucleons) the following equation on $|U_1\rangle$:

$$(1 - V_1 G_0) |U_1\rangle = V_1 G_0 P |U_1\rangle + V_4^{(1)} G_0 (1 + P) |U_1\rangle + \mathcal{O}_1 |\Psi_0\rangle, \tag{9}$$

where P is the sum of a cyclical and anticyclical permutation of 3 particles. Using the identities for the NN t-operator t_1

$$(1 - V_1 G_0)^{-1} = 1 + t_1 G_0,$$

$$(1 - V_1 G_0)^{-1} V_1 G_0 = t_1 G_0$$
(10)

we obtain the final Faddeev-like equation on $|U_1\rangle$:

$$|U_1\rangle = (1 + t_1 G_0) \mathcal{O}_1 |\Psi_0\rangle + (t_1 G_0 P + (1 + t_1 G_0) V_4^{(1)} (1 + P) G_0) |U_1\rangle.$$
 (11)

The response function R_T is then obtained as

$$R_T(E_\gamma) = -\frac{3}{\pi} \Im \langle \Psi_0 | \mathcal{O}_1^{\dagger} (1+P) G_0 | U_1 \rangle, \tag{12}$$

where \mathcal{O} is taken as the transverse current operator of Ref. [15]

The response function R_T can also be obtained by means of direct integrations in Eq. (2). This gives not only a possibility for a check of numerics, but provides information about two– and three–body parts of the total cross section.

B. The Lorentz Integral Transform Method

In the LIT approach the need to compute final state continuum wave functions is avoided [13]. In fact the response function R_T is obtained via evaluation and subsequent inversion of its LIT

$$L(\sigma_R, \sigma_I) = \int_{E_{th}}^{\infty} dE_{\gamma} \frac{R(E_{\gamma})}{(E_{\gamma} - \sigma_R)^2 + \sigma_I^2}.$$
 (13)

Neglecting the small recoil term in Eq. (2) $E_{\gamma} = E_f - E_0$ and applying closure the transform $L(\sigma)$ of the response R_T is found as

$$L(\sigma_R, \sigma_I) = \langle \tilde{\Psi}(\sigma_R, \sigma_I) | \tilde{\Psi}(\sigma_R, \sigma_I) \rangle, \tag{14}$$

where $\tilde{\Psi}$ is the localized solution of the Schrödinger-like equation

$$(H - E_0 - \sigma_R + i\sigma_I)\tilde{\Psi} = Q \tag{15}$$

with the source term $Q = \mathbf{J}_T \Psi_0$. The wave function Ψ_0 is the ground state solution for the same hamiltonian.

In order to calculate Ψ_0 and $\tilde{\Psi}$ expansions on correlated hyperspherical harmonics (CHH) are used

$$\Psi = \tilde{\Omega} \sum_{i} c_{i} \phi_{i}, \qquad (16)$$

where $\tilde{\Omega}$ is a correlation operator and ϕ_i is a totally antisymmetric basis set constructed from a spatial part $\chi_{i,\mu}$ and a spin-isospin part θ_{μ}

$$\phi_i = \sum_{\mu} \chi_{i,\mu} \theta_{\mu} . \tag{17}$$

The operator $\tilde{\Omega}$ is a state dependent correlation operator. Further details can be found in Ref. [6]. Calculating $L(\sigma_R, \sigma_I)$ for a sufficient number of σ_R and fixed σ_I , one obtains R_T from the inversion of the LIT (for details of the inversion see Ref. [14])

C. Comparison between the two Approaches

It is evident that the Faddeev and LIT methods are completely different. The Faddeev results are obtained essentially by solving Eq. (11) in momentum space while the LIT results are obtained by first solving Eq. (15) in configuration space and then inverting Eq. (13) with $L(\sigma)$ given by Eq. (14). Therefore the comparison between the results obtained with the two methods is a very significant test of accuracy reached by these approaches.

There is an interesting similarity between the two methods, namely, the fact that closure plays an important role in both approaches. Indeed it is just the use of closure that leads to Eqs. (5) and (15), respectively. Actually these two equations are equal provided that $\sigma_I \to \epsilon$. However in the LIT case the finite σ_I in Eq. (15) effectively makes it a bound state problem, while the Faddeev-like equation (11) remains a continuum problem.

In judging the quality of agreement between the results of the two methods one has to take into account that the LIT results are obtained in the "unretarded dipole approximation". In the following we recall this approximation briefly. It consists in replacing the total current operator $\mathbf{J}(\mathbf{Q})$ by its limit $\mathbf{J}(Q=0)$. Then one makes use of the continuity equation

$$\mathbf{Q} \cdot \mathbf{J}_{f0}(\mathbf{Q}) = E_{\gamma} \,\rho_{f0}(\mathbf{Q}) \,, \tag{18}$$

where $\rho(\mathbf{Q})$ represents the charge operator. Expanding $\rho_{f0}(\mathbf{Q})$ in powers of \mathbf{Q} and taking into account that $\rho_{f0}(Q=0)=0$, one gets

$$\mathbf{Q} \cdot \mathbf{J}_{f0}(Q=0) = E_{\gamma} \mathbf{Q} \cdot \left[\left(\vec{\nabla}_{\mathbf{Q}} \rho \right)_{Q=0} \right]_{f0}. \tag{19}$$

As the direction of \mathbf{Q} is arbitrary, one has

$$\mathbf{J}_{f0}(Q=0) = E_{\gamma} \left[\left(\vec{\nabla}_{\mathbf{Q}} \rho \right)_{Q=0} \right]_{f0}. \tag{20}$$

Since the gradient of ρ for Q=0 is the dipole operator one writes

$$\left[\left(\vec{\nabla}_{\mathbf{Q}} \rho \right)_{Q=0} \right]_{f0} = i \mathbf{D}_{f0} . \tag{21}$$

Thus Eq. (1) becomes the well known result for the photonuclear cross section in unretarded dipole approximation

$$\sigma = 4\pi^2 \frac{e^2}{\hbar c} E_{\gamma} R_D(E_{\gamma}) \tag{22}$$

with

$$R_D(E_\gamma) = \int df \, |\langle \Psi_f | \mathbf{D} | \Psi_0 \rangle|^2 \, \delta(E_\gamma - E_f + E_0) \,. \tag{23}$$

For the LIT only R_D is calculated. Since our energy range of interest is below pion threshold the unretarded dipole approximation should be very good. In the following discussion a check of this assumption will be presented in the framework of the momentum space Faddeev approach. In this framework one can use the representation of the electric multipoles of the transition operator obtained in Ref. [15] employing the continuity equation (18) with $E_{\gamma} = Q$:

$$T_{J\varepsilon}^{el}(Q) = T_{J\varepsilon}^{\rho} + T_{J\varepsilon}^{res}, \qquad (24)$$

$$T_{J\xi}^{\rho} = -\frac{1}{4\pi} \sqrt{\frac{J+1}{J}} \int d\hat{Q} Y_{J\xi}(\hat{Q}) \rho_{f0}(\mathbf{Q}),$$
 (25)

$$T_{J\xi}^{res} = -\frac{1}{4\pi} \sqrt{\frac{2J+1}{J}} \int d\hat{Q} \left(\mathbf{Y}_{J,J+1,1}^{\xi}(\hat{Q}) \cdot \mathbf{J}_{f0}(\mathbf{Q}) \right) . \tag{26}$$

Here $\xi = \pm 1$ and $\mathbf{Y}_{J,J+1,1}^{\xi}$ are vector spherical harmonics. In the limit $Q \to 0$ the contribution (26) behaves as Q^{J+1} , while the contribution (25) behaves as Q^J . Expressing $T_{J\xi}^{\rho}$ in terms of the density matrix elements $\rho_{f0}(\mathbf{R})$ one finds that

$$\lim_{Q \to 0} \left[Q^{-J} T_{JM}^{el}(Q) \right] = \lim_{Q \to 0} \left[Q^{-J} T_{JM}^{\rho}(Q) \right] = -i^{J} \sqrt{\frac{J+1}{J}} \frac{1}{(2J+1)!!} \int d\mathbf{R} R^{J} Y_{JM}(\hat{R}) \rho_{f0}(\mathbf{R}) ,$$
(27)

which is known as Siegert's theorem, namely that the electric multipole transitions are completely determined via the charge density in the limit $Q \to 0$. In particular, for J = 1 one has

$$(D_M)_{f0} = i\sqrt{6\pi} \lim_{Q \to 0} \left[Q^{-1} T_{1M}^{\rho}(Q) \right] . \tag{28}$$

This is the relation which has been used in the framework of the Faddeev calculation to test the quality of the unretarded E1 approximation.

Corrections to the unretarded E1 approximation consist of two parts. The first part is due to the difference between $T_{1M}^{\rho}(Q)$ of Eq. (25) and its limit for $Q \to 0$. We shall refer to this correction as a retardation correction. The second part is $T_{J\xi}^{res}$ of Eq. (26). It is seen from above that both corrections vanish at small Q. Additional contributions come from magnetic multipoles (see Eq. (4) in [15]) and higher EJ multipoles.

III. RESULTS AND DISCUSSION

For the calculation of the total photoabsorption cross section σ_T we use the AV18 NN interaction [16], the 3-body force Urbana IX [17] and for the LIT case also the Coulomb force. Only the unretarded dipole approximation R_D is considered within the LIT method. The Faddeev results also include retardation effects, additional multipoles of the usual one-body current and explicit MEC.

We start the discussion with the benchmark test. In Fig. 1 the comparison between LIT and Faddeev results is presented in unretarded dipole approximation without (Fig. 1a) and with (Fig. 1b) the 3N force. There are two curves for the LIT case showing the small uncertainties in the inversion of the transform. Besides small differences at higher energies the agreement between the two methods is excellent for AV18. Inclusion of the 3N force gives slightly poorer agreement in the peak region and at the low energy side of the peak, where the two curves have a relative shift of 0.2 MeV. We do not think that this small difference is of relevance at present; only in case of future high precision experiments would it be reconsidered. Fig. 1b shows also the result for AV18 only. As already pointed out in Refs. [6,7] one finds a decrease of the peak and enhancement of the tail due to the 3N force.

In Fig. 2 we show the retardation effects (Fig. 2a) and those due to the additional contributions of $T_{1\xi}^{res}$ and of magnetic and higher electric multipoles (Fig. 2b). Only the one-body current was employed to calculate these additional contributions. One sees that the retardation effects reduce the cross section. They are very small below 50 MeV (1 % or less) and become somewhat more sizable at higher energies (5 % at 100 MeV, 17 % at pion threshold). As seen in Fig. 2b the increase due to additional multipoles is rather similar with and without 3N force. Only beyond 80 MeV does the difference become somewhat more pronounced. At low energy there is a tiny decrease due to the additional E1 contribution. Above 30 MeV the higher multipole contributions are increasing up to 30 % at pion threshold.

It is interesting to note that one finds a partial compensation of retardation and higher multipole effects as predicted by Gerasimov via sum rule considerations [18].

In Fig. 3 we illustrate the effect of the Coulomb force in the threshold region. The neglect of the Coulomb force leads to an increase of the cross section close to threshold (about 10 % at 7 MeV), but becomes rather small beyond 15 MeV. Considering the Coulomb force only in the ground state is not a good approximation. It is better to neglect the Coulomb force completely.

Now we turn to the discussion of MEC effects. Generally it is a problem to construct a consistent exchange current for a given NN potential. Using, however, minimal coupling one obtains a MEC with the correct divergence of the current also in case of realistic NN potentials [9,19], while the rotor of the current remains model dependent. Here we use only the standard π - and ρ -like exchange currents for AV18, which are determined according to the Riska prescription [19]. In the present Faddeev calculation MEC are added to the onebody current without making a multipole decomposition, therefore without using Eq. (24). This differs from the usual approach where the gauge condition Eq. (18) is applied to obtain a representation similar to that of Eq. (24) and thus only MEC contributions beyond it are calculated explicitly. Such a procedure has the advantage that one violates gauge invariance in the minimal way since the divergence of the full current is taken into account correctly. For example, in a calculation with 3N forces one automatically takes into account a large part of three–nucleon MEC effects. Fig. 4 illustrates that the result with explicit MEC differs rather substantially from that with one-body current and implicit MEC via Siegert's theorem. This suggests that the MEC are not fully consistent with the potential. Indeed, using Eq. (24) for a current satisfying the continuity equation the explicit MEC contribution to the E1 multipole would manifest itself only in the residual term (26) which vanishes for $Q \to 0$. Even away from this limit $T_{J\xi}^{res}$ is probably small, as it is in the case of the deuteron [20]. In addition, MEC contributions to other multipoles could not decrease the cross section, since the cross section is the incoherent sum of all multipoles and without explicit MEC such multipole contributions are negligible at low energies (see Fig. 2b).

The contributions of the two- and three–body break up channels are shown in Fig. 5a. The three-body break up cross section becomes larger than that of the two-body break up already at 14 MeV and at higher energies it is the dominating channel. In Fig. 5b we compare the total three–body break up cross section with that of the final isospin T=3/2 channel (which is three–body break up exclusively). It is interesting to see that at low energy the T=1/2 channel gives a small contribution to the three body break up, while it becomes increasingly important at higher energies.

In Fig. 6 we compare the triton results with experimental data. One finds a rather good agreement between theory and experiment at low energy for both channels. Since the experimental situation at higher energy is not settled, a definite comparison between theory and experiment cannot be made. In fact the two-body break up data are rather scattered and there is limited experimental information on the three-body break up.

In Fig. 7 we compare the total ³He cross section with data (the results for ³H with AV18 and UrbIX are presented in [7]). One finds a rather good agreement between theoretical and experimental data and it is evident that the 3N force improves the comparison with experiments at low energy. On the other hand due to the insufficient precision of the experimental data a more conclusive comparison between theory and experiment cannot be

made.

We summarize our results as follows. Benchmark results of high precision have been set for the three–nucleon total photoabsorption cross sections. The theoretical quality of the results is considerably higher than the experimental uncertainties. Of course, one has to take into account that these experimental data are rather old. Thus new experimental activity in this field would appear to be timely. The classical approximation for photonuclear cross sections, i.e. the unretarded dipole approximation, is extremely good below 50 MeV. It is also rather good at even higher energies (error at 100 MeV below 20 %), since one has a partial cancellation of the E1 retardation effects and contributions from additional multipoles. The Coulomb force effects on the cross section become negligible about 6-7 MeV above threshold but are important at lower energy.

Acknowledgement

Parts of this work were supported by the Deutsche Forschungsgemeinschaft (J.G.), the Polish Committee for Scientific Research (grant 2P03B02818), a NATO Collaborative Research Grant (W.L.,G.O.,E.L.T.), the National Science and Engineering Research Council of Canada (E.L.T.), the Russian Fund for Basic Research, grant 00–15–96590 (V.D.E.), and the Italian Ministry of Research (V.D.E.,W.L.,G.O.). A.N. acknowledges partial support from NSF grant #PHY0070858. Parts of the numerical Faddeev calculations have been performed on the Cray T90 and T3E of the NIC in Jülich, Germany.

REFERENCES

- [1] I.M. Barbour and A.C. Phillips, Phys. Rev. C1 (1970) 165.
- [2] B.F. Gibson and D.R. Lehmann, Phys. Rev. C 11 (1975) 29; 13 (1976) 477.
- [3] K.K. Fang, J.S. Levinger, and M. Fabre de la Ripelle, Phys. Rev. C 17 (1978) 24.
- [4] A.N. Vostrikov and M.V. Zhukov, Yad. Fiz. 34 (1981) 344 [Sov. J. Nucl. Phys. 34, 196 (1981)].
- [5] V.D. Efros, W. Leidemann, and G. Orlandini, Phys. Lett. B408 (1997) 1.
- [6] V.D. Efros, W. Leidemann, G. Orlandini, and E.L. Tomusiak, Phys. Lett. B484 (2000) 233.
- [7] V.D. Efros, W. Leidemann, G. Orlandini, and E.L. Tomusiak, Nucl. Phys. A689 (2001) 421c.
- [8] H. Arenhövel, W. Fabian, and H.G. Miller, Phys. Lett. **B52** (1974) 303.
- [9] A. Buchmann, W. Leidemann, and H. Arenhövel, Nucl. Phys. A443 (1985) 726.
- [10] H. Arenhövel and M. Sanzone, Few-Body Syst. Suppl. 3 (1991).
- [11] J. Golak, H. Witała, H. Kamada, D. Hüber, S. Ishikawa, and W. Glöckle, Phys. Rev. C 52 (1995) 1216.
- [12] S. Ishikawa, J. Golak, H. Witała, H. Kamada, W. Glöckle, and D. Hüber, Phys. Rev. C 57 (1998) 39.
- [13] V.D. Efros, W. Leidemann, and G. Orlandini, Phys. Lett. B 338 (1994) 130.
- [14] V.D. Efros, W. Leidemann, and G. Orlandini, Few-Body Syst. 26 (1999) 251.
- [15] J. Golak et al., Phys. Rev. C **62** (2000) 054005.
- [16] R.B. Wiringa, V.G.J. Stoks, and R. Schiavilla, Phys. Rev. C 51 (1995) 38.
- [17] R.B. Wiringa, Phys. Rev. C 43 (1991) 1585; B.S. Pudliner, V.R. Pandharipande,
 J. Carlson, C. Steven Pieper, and R.B Wiringa, Phys. Rev. C 56 (1997) 1720.
- [18] S.B. Gerasimov, Phys. Lett. **13** (1964) 240.
- [19] D.O. Riska, Phys. Scr. **31** (1985) 107; **31** (1985) 471.
- [20] H. Arenhövel, Z. Phys. A **302** (1981) 25.
- [21] R.B. Bösch, J. Lang, R. Müller, and W. Wölfli, Phys. Lett. 8 (1964) 120; Helv. Phys. Acta 38 (1965) 753.
- [22] R. Kosiek, D. Müller, and R. Pfeiffer, Phys. Lett. **21** (1966) 199.
- [23] D.D. Faul, B.L. Berman, P. Meyer, and D. Olson, Phys. Rev. C 24 (1981) 849.
- [24] D.M. Skopik, D.H. Beck, J. Asai, and J.J. Murphy II, Phys. Rev. C 24(1981) 1791.
- [25] G. Mitev, P. Colby, N.R. Roberson, and H.R. Weller, Phys. Rev. C **34**(1986) 389.
- [26] J. Mösner, K. Möller, W. Pilz, G. Schmidt, and T. Stiehler, Few-Body Syst. 1 (1986) 83.
- [27] V.N. Fetisov, A.N. Gorbunov, and A.T. Varfolomeev, Nucl. Phys. A71 (1965) 305.

FIGURES

- FIG. 1. Comparison of the Faddeev and LIT results for the total ³H photoabsorption cross section in unretarded dipole approximation without (a) and with (b) 3N force. The dots are the Faddeev results and the two curves represent the bounds for the inversion of the LIT. The dotted curve in (b) is the result with AV18 only.
- FIG. 2. (a) Retardation effects to the unretarded E1 triton cross section $(\sigma_{ret} \sigma_{unret})/\sigma_{unret}$ and (b) retardation and additional contributions (see text) $(\sigma_{tot} \sigma_{unret})/\sigma_{unret}$.
- FIG. 3. Relative effect of the Coulomb force on the ³He photoabsorption cross section: no Coulomb at all, i.e. triton result with shifted threshold (dashed curve), no Coulomb in final state interaction (dotted curve).
- FIG. 4. ³He photoabsorption cross section without a 3N force for the full one-body current and implicit MEC contribution via application of Eq. (24) (magnetic one-body transitions considered via Eq. (4) of Ref. [15]) (full dots) and result for the full one-body current with additional explicit MEC but without application of Eq. (24) (empty dots). Curves are spline interpolations.
- FIG. 5. (a) Two-body (dotted curve), three-body (dashed curve) and total (full curve) break up cross sections of the ³H photodisintegration (full one-body current and implicit MEC contribution as in Fig. 4). (b) Comparison of the total three-body break up cross section (dashed curve) with the cross section in the final state isospin channel T=3/2 in the unretarded dipole limit.
- FIG. 6. Two-body (a) and three-body (b) break up cross sections for the ³H photodisintegration (full one-body current and implicit MEC contributions as in Fig. 4). The full curves represent Faddeev results. Experimental data in (a) from [21] (circles), [22] (squares), [23] (diamonds), [24] (triangles up), [25] (triangles down), [26] (X). The dotted lines in (b) are bounds of experimental data from [23].
- FIG. 7. Total ³He photoabsorption cross section. LIT results in unretarded dipole approximation with AV18 alone (dash-dotted curve) and with AV18+UrbIX (full curve); the dotted lines are bounds of experimental data from [23] and the dots are data from [27].

Fig. 1

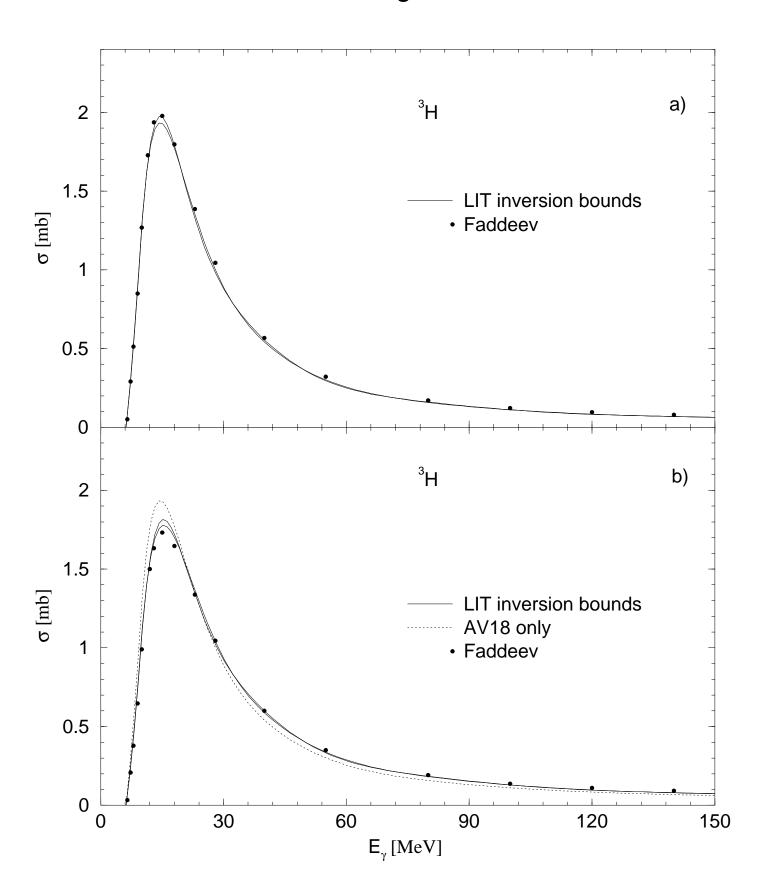


Fig. 2

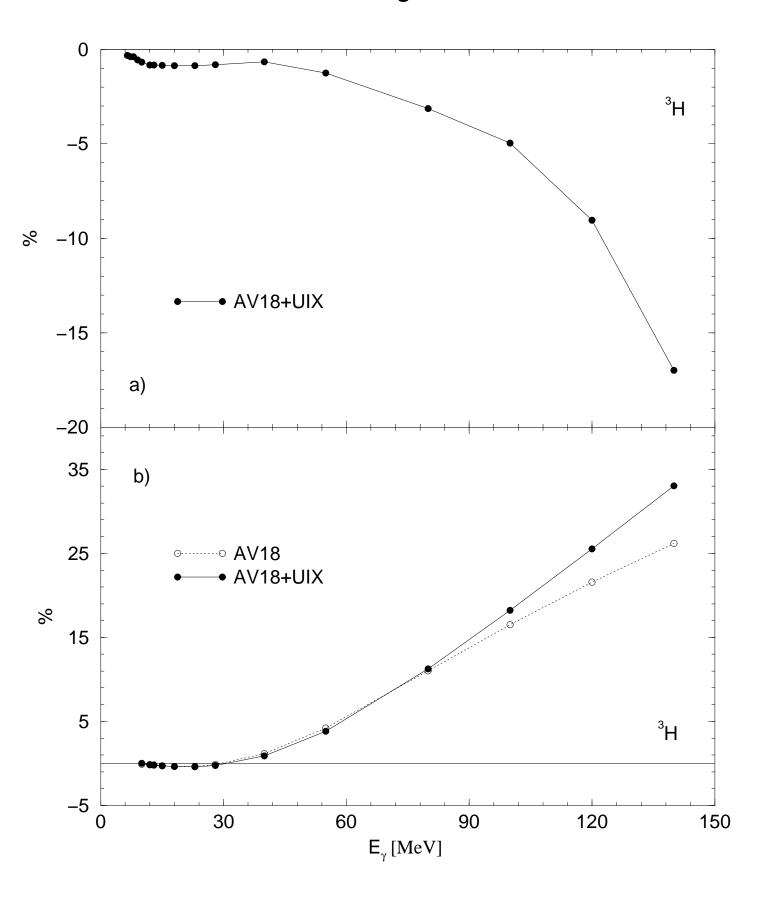


Fig. 3

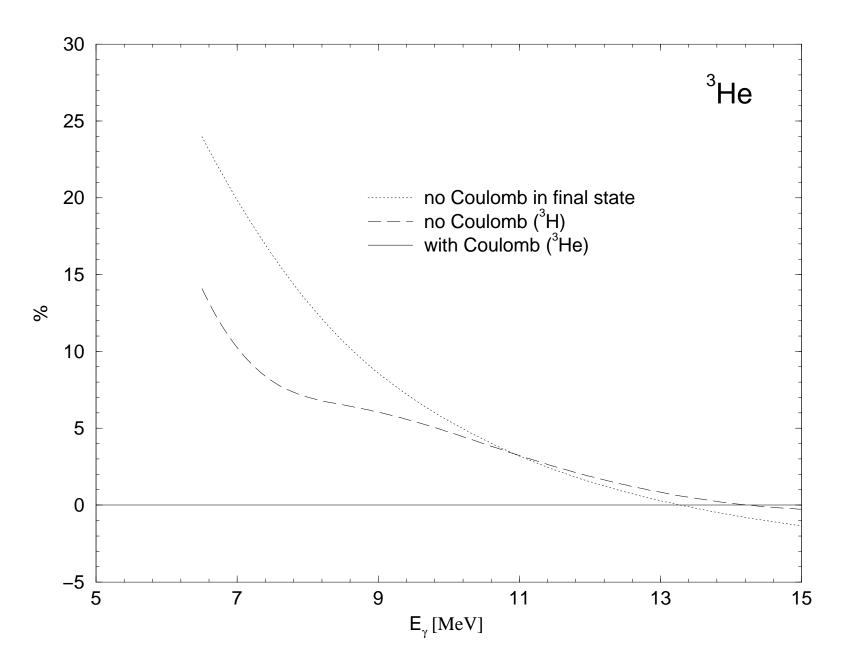


Fig. 4

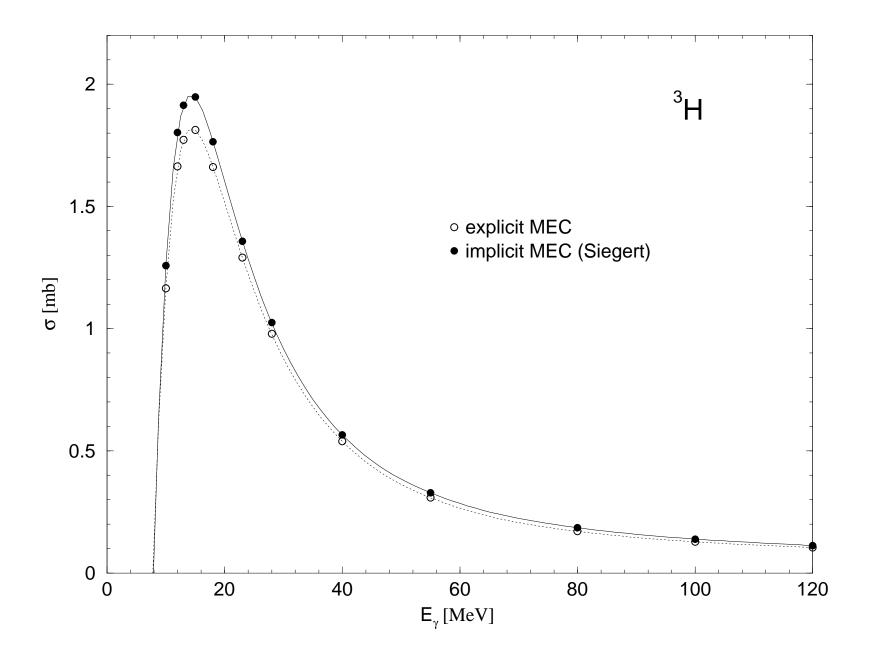


Fig. 5

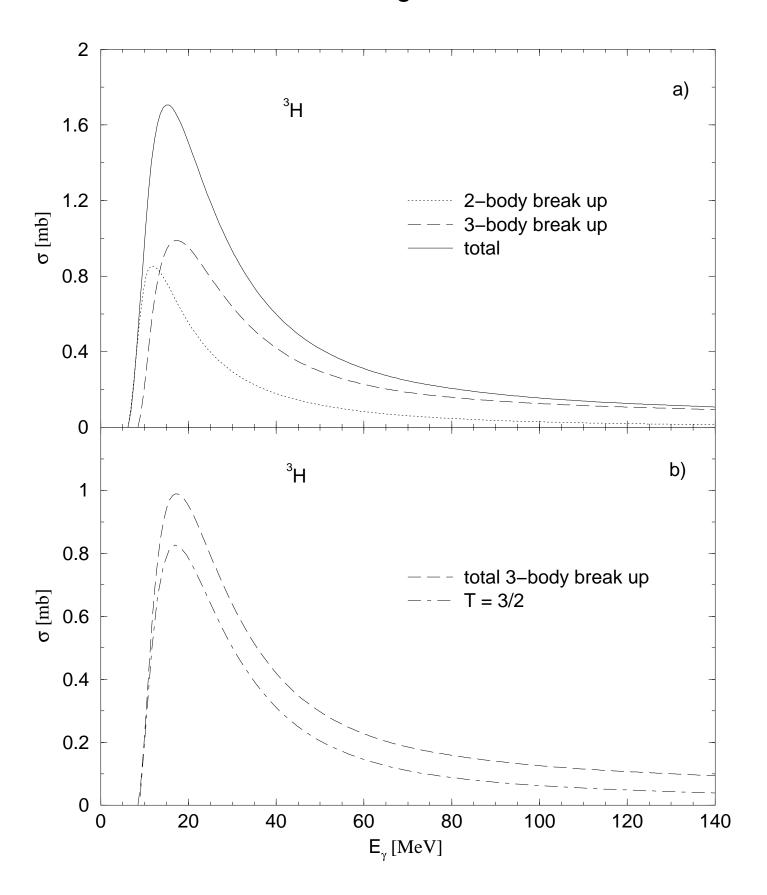


Fig. 6

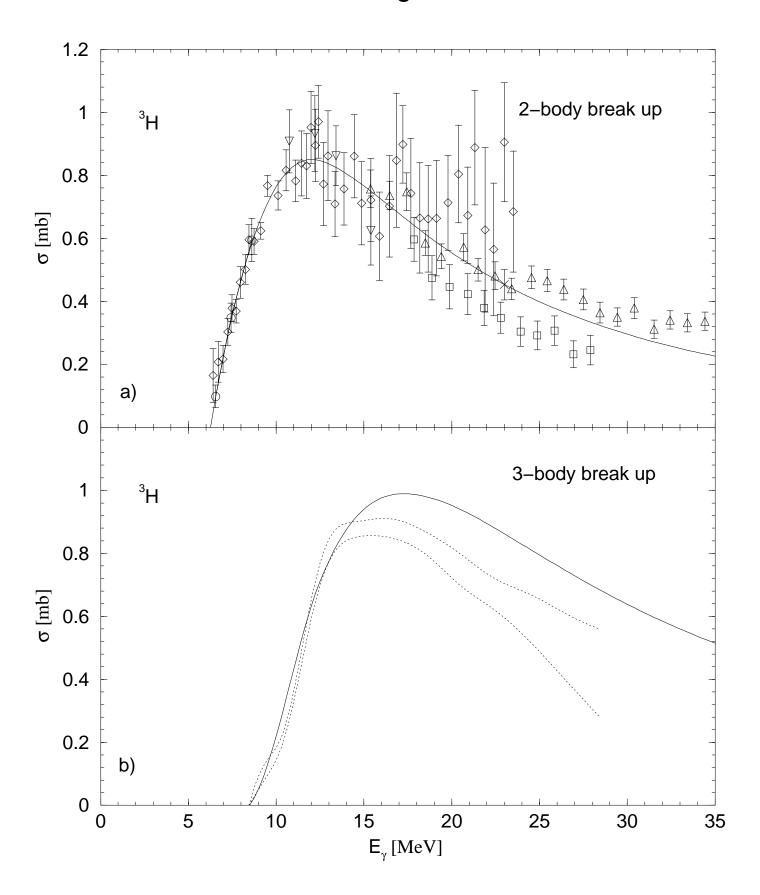


Fig. 7

